Vietnam Journal of Catalysis and Adsorption
Tạp chí xúc tác và hấp phụ Việt Nam

https://jca.edu.vn

Synthesis of visible light active $GdFeO_3$ photocatalyst for photo-Fenton degradation of Indigo Carmine dye

Thi To Nga Phan[1*], Manh Duc Nguyen[1], Doan Ngoc Linh Giang[2]

[1]*School of Chemistry and Life Sciences, Hanoi University of Science and Technology*
[2]*Taylor's College, Malaysia*
**Email: nga.phanthito@hust.edu.vn*

ARTICLE INFO

Received: 15/3/2023
Accepted: 25/6/2023
Published: 30/3/2024

Keywords:
$GdFeO_3$, hydrothermal method, photo-Fenton, degradation, dye

ABSTRACT

Perovskite $GdFeO_3$ were prepared by a facile hydrothermal method and used as a visible-light-responsive photocatalyst. The as-prepared $GdFeO_3$ photocatalyst was characterized by X-ray Diffraction (XRD), scanning electron microscopy (SEM), transmission electron microscopy (TEM), N_2 adsorption-desorption, and Ultraviolet–Visible Diffuse Reflectance Spectroscopy (UV-vis DRS). The photo-Fenton catalytic activities of perovskite $GdFeO_3$ were investigated for the degradation of Indigo Carmine. The results showed that $GdFeO_3$ photocatalyst had a good performance under visible light irradiation. The remarkable enhancement photo-Fenton catalytic activity of $GdFeO_3$ material could be attributed to its small particle size and narrow band gap energy.

1. Introduction

Synthetic organic dyes such as indigo carmine (IC) have been used to accommodate the expanding demand in the textile industry and 20% of the total dyes were discharged into the water bodies during the dyeing process [1], which causes serious impacts on aquatic life and human wealth. Several methods have been developed to remove dyes from wastewater, including adsorption [2], biological [3], ozonation [4], and filtration methods [5]. However, they are having problems with high expenses and more concentrated byproducts (the contaminants have not undergone a drastic purification). As an alternative, heterogeneous photo-Fenton catalysis, an advanced oxidation process, functions as a destructive technology, causing the full mineralization of the majority of organic pollutants in order to prevent the production of toxic degradation products (such as aromatic amines, which are human cancer-causing substances) [6]. Whereas, the classical Fenton oxidation process utilizes the reaction between Fe(II)/Fe(III) and hydrogen peroxide to generate hydroxyl radicals (▪OH), which can oxidize organic pollutants in wastewater [7]. The use of UV light or visible light irradiation could further accelerate the Fenton process; such usually refer to as the photo-Fenton reaction [8]. Recently, numerous Fe-containing rare earth metal oxides have been demonstrated for usage as heterogeneous photo-Fenton catalysts [9]. Particularly, $GdFeO_3$ (GFO) exhibits favorable properties as a member of the ABO_3 perovskite family. For example, GFO, having a strong stability in liquid phase, can function under visible light illumination due to its low band gap energy [10]. Several synthetic methods have been made to synthesize ABO_3, such as solid state [11], co-precipitation [12], sol-gel method [13], hydrothermal synthesis [14], and self-combustion [15]; in which the hydrothermal method is promising because of low temperature, cost effectiveness and process simplicity.

https://doi.org/10.62239/jca.2024.020

Until now, only a few studies have reported on the preparation of ABO_3 *via* hydrothermal method and its application in the photo-Fenton process aiming at dye degradation under visible light irradiation. For instance, Alpay and co-workers [16] have successfully prepared $LaFeO_3$ on polystyrene resin by employing hydrothermal method and found that the synergistic effect of adsorption and photo-Fenton reaction significantly influenced the photo-Fenton catalytic efficiency [16]. Their results showed that about 60% of Indigo Carmine in 50 mL of 10 mg/L solution was degraded within 170 mins in the presence of H_2O_2 10mM and 0.01 g catalyst under visible light irradiation. The Cu-doped $LaFeO_3$ particles, which were hydrothermally synthesized by Parrey, could effectively degrade Methyl Orange (MO) [17]. The removal efficiency of tetracycline reached 70 % after 2 h exposure to visible light under the initial reaction conditions of 2 mL H_2O_2 35 w/v%, 0.1 g catalyst and 80 ml MO. However, to the best of our knowledge, no study has been performed on the application of GFO, synthesized *via* hydrothermal method, as heterogeneous photo-Fenton-like catalyst for Indigo Carmine degradation; which was the objective of this study. Herein, we studied the structural, morphological and optical properties of hydrothermally synthesized GFO. The photo-Fenton- catalytic activity of our as-synthesized GFO was evaluated towards the degradation of Indigo Carmine (IC), which was selected as the dye model, under visible light. It was then optimized in terms of catalyst loading, initial solution pH and initial H_2O_2 dosage.

2. Materials and Methods

Materials

Gadolinium nitrate hexahydrate ($Gd(NO_3)_3{\cdot}6H_2O$; 99.9%), Iron nitrate nonahydrate ($Fe(NO_3)_3{\cdot}9H_2O$; 98 %), citric acid ($C_6H_8O_7{\cdot}H_2O$; ≥99.5%), Indigo Carmine (IC; ≥85%), hydrogen peroxide solution (H_2O_2, 30%), and ammonium hydroxide solution (NH_4OH, 30%) were purchased from Sigma-Aldrich. All chemicals were analytical grade and used as received without further purification.

Synthesis of $GdFeO_3$

In the hydrothermal synthesis of $GdFeO_3$ (GFO), 0.005 mol of $Gd(NO_3)_3{\cdot}6H_2O$, 0.005 mol of $Fe(NO_3)_3{\cdot}9H_2O$, and 0.01 mol of citric acid (a chelating agent) were dissolved in 10 mL of deionized (DI) water. The mixture was stirred for 2 h at ambient temperature. Then, ammonium hydroxide solution was dropped to the mixture to adjust solution pH to 9, following by stirring for another 1 h. Afterwards, the resulting synthetic solution was transferred to a 50 mL Teflon-lined autoclave and heated at 180 °C for 20 h. The solids were separated by centrifugation, washed with DI water and ethanol, dried at 80 °C overnight and finally calcined at 800 °C for 6 h in air. The resulting sample was named as GFO [8].

Characterizations of photocatalyst

X-ray powder diffraction (XRD) pattern of GFO was measured on D8 Advance - Bruker diffractometer with Cu-Kα radiation with wavelength λ=1.54065 Å, scanning speed 0.02^0/s, 2θ range from 10^0 to 80^0. The surface morphology of the material was investigated by scanning electron microscopy (SEM) on the Zeiss 1555 VP-FESEM. Transmission electron microscopy (TEM) was measured on H7500, HITACHI. Fourier transform infrared (FTIR) spectra were recorded on a FTIR spectrometer (JASCO FT/IR-4600) using the KBr pellet technique. Nitrogen adsorption-desorption isotherm was conducted at 77K on MICROMERITICS 2020. Ultraviolet diffuse reflectance spectroscopy was measured on LAMBDA 750 UV/Vis/NIR system, PerkinElmer.

Photo-Fenton catalytic degradation of IC

Photo-Fenton catalytic activity of the sample was evaluated by adding GFO into 100 mL of 10 mg/L IC aqueous solution in a double wall glass reactor, which was surrounded by a circulating water jacket to maintain solution temperature at room temperature. Prior to photo-Fenton process, the suspension was magnetically stirred in dark for 30 min to reach an adsorption-desorption equilibrium of IC onto GFO. A photo-Fenton reaction was started by adding 1 mL H_2O_2 30% to the suspension along with turning on a Xenon lamp (CEL-HX F300) with a 400 nm cut-off filter to provide visible light for photo-Fenton degradation test. After that, 4 mL of the sample was taken from the suspension every 15 min and centrifuged for separation; the obtained supernatant was tested using Perkin Elmer Lambda 750 UV/Vis spectrometer to confirm the concentration of IC. The photo-Fenton degradation rate % was calculated using formula given below:

$$Degradation\ rate\ (\%) = \left(1 - \frac{C_t}{C_0}\right) \times 100\%$$

https://doi.org/10.62239/jca.2024.020

where C_0 and C_t are the IC concentrations before degradation and during degradation at a given period of time, respectively.

3. Results and discussion

Characterizations

Fig. 1 shows the XRD patterns of GFO. The observed characteristic diffraction peaks appearing at 23.1°, 25.8°, 32.1°, 32.9°, 33.5°, 34.1°, 39.1°, 40.2°, 41.2°, 42.5°, 47.4°, 48.7°, 53.4°, 57.5°, 58.4°, 59.6°, 64.2°, and 69.4° correspond to (110), (111), (200), (121), (002), (210), (1121), (220), (022), (131), (202), (212), (311), (321), (240), (123), (331), and (242) facets of orthorhombic phase $GdFeO_3$, respectively (JCPDS no. 47-0067) [18]. No other impurity diffraction peaks are observed in Fig. 1, confirming high purity of GFO. The average crystallite size of GFO is 29.4 nm, which was calculated based on the characteristic peak of (121) plane in Fig. 1 and the Debye-Scherrer formula [19].

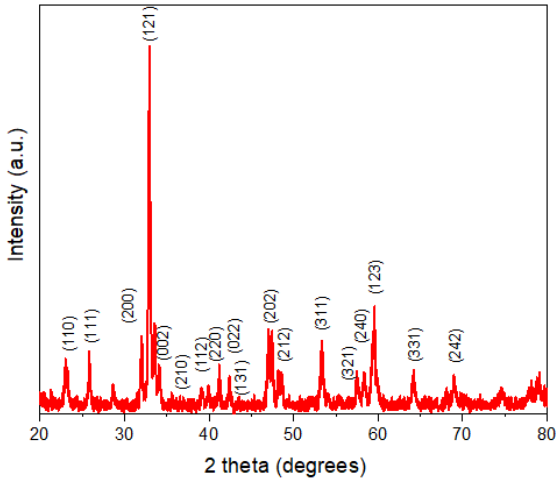

Fig 1: XRD pattern of GFO

Fig. 2a shows the SEM image of GFO. As can be seen from Fig. 2a that GFO sample showed the spherical-like particles with agglomeration. It is also possible to see small particles accumulated on to the surfaces of GFO. This interesting finding could be attributed to the dissolution-recrystallization process during the hydrothermal treatment.

TEM image of GFO in Fig. 2b provided further insight in its morphology. Obviously, the sample consisted of spherical-like particles which were formed by agglomerated spherical particles with the average particle size of around 50 – 80 nm. The structural properties of GFO such as BET (Brunauer Emmett Teller) specific surface area, pore size, and pore volume were listed in Table 1. The low specific surface area of GFO could be ascribed to the limitation of conventional preparation method such as hydrothermal method [21]. Meanwhile, the presence of pores in GFO sample could be attributed to the pores formed between the particles due to aggregation.

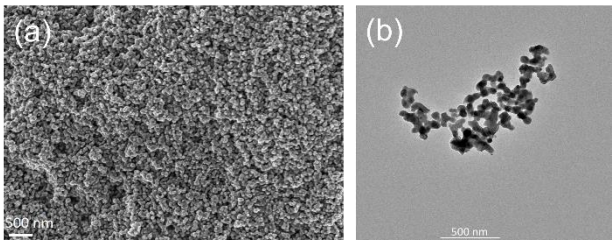

Fig 2: (a) SEM image and (b) TEM image of GFO

Table 1: Structural property of GFO sample

Sample	S_{BET} (m^2/g)	Pore volume (cm^3/g)	Average pore size (nm)
GFO	10.51	0.09	39.81

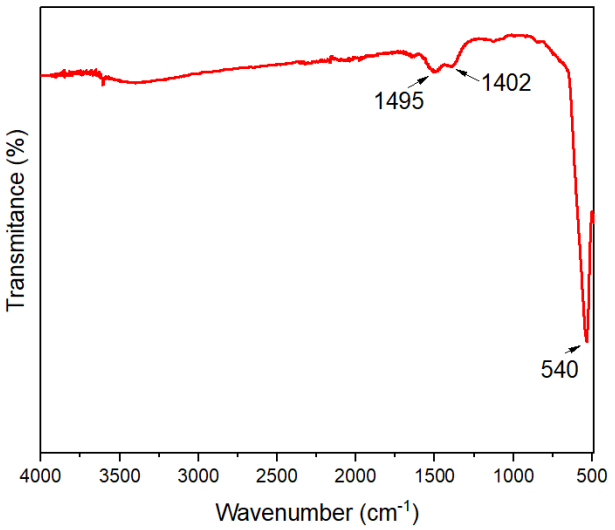

Fig 3: Fourier transform infrared spectra of the GFO nanoparticles

Fig. 3 reveals FTIR spectra of GFO sample in the range from 4000 - 400 cm^{-1}. As can be seen clearly from Fig. 3 that the asymmetric stretching of carbonates have been reported at 1495 and 1402 cm^{-1}, respectively, suggesting that carbonate species form on the GFO surface [19]. However, the presence of the species cannot be detected by XRD analysis. From the literature survey, the sharp peaks of Fe-O stretching bands at 540 cm^{-1} which are characteristics of the octahedral FeO_6 group in GFO have assigned to the formation of GFO [8]. These observations agree with the results obtained from XRD pattern that the single crystalline NFO phase has already been formed at 800 °C.

https://doi.org/10.62239/jca.2024.020

In order to evaluate the optical property of the GFO samples, the diffuse reflectance spectra of the sample were measured and shown in Fig. 4. It is easy to see that GFO photocatalyst sample exhibited strong absorption peaks in the visible region (400 - 800 nm), as shown in Fig. 4. The optical band gap of the material can be determined from the reflectance spectral data according to the Kubelka-Munk equation. The optical band gap is determined based on the relationship between hν (energy corresponding to each wavelength) and the coefficient α, which depends on F(R) – the Kubelka-Munk function according to the expression [20]:

$$F(R) = \frac{(1-R)^2}{2R} \quad (1)$$

where F(R) is Kubelka-Munk function and R is reflectance. The relationship between $[(F(R).h\nu)^2]$ and hν in the allowed direct electron transition is shown in the inset of Fig. 4. The optical band gap energy of the GFO was 2.20 eV. The narrow band gap energy of the catalyst sample indicated that the GFO catalyst can act as photocatalyst activating in the visible light region.

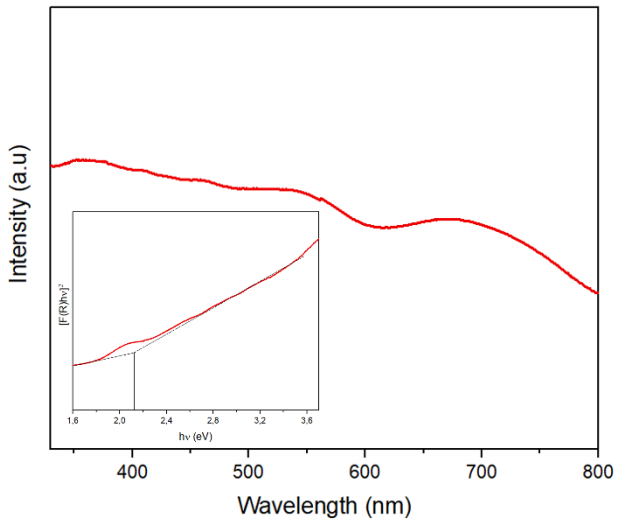

Fig 4: (a) UV-Vis absorption spectra of GFO and inset is the plot of $(F(R)h\nu)^2$ versus hν

Photo-Fenton degradation of IC

The photo-Fenton catalytic performance of GFO was tested by the degradation of IC in the presence of H_2O_2 and visible light. Prior to starting visible light irradiation, the adsorption of IC onto GFO was found negligible, which was approximately 1%. It is possible to see from Fig. 5, the GFO sample showed good catalytic performance for IC Fenton-degradation under visible light irradiation with 98.5 % of IC removed after 90 min, which is significantly greater than 65 % of IC removed by GFO in the absence of H_2O_2. It is worth noting that when no catalyst was added, the degradation of IC was only ~3% under visible light irradiation only (photolysis) and 9% in the presence of H_2O_2 after 90 min visible light irradiation (H_2O_2/photolysis) (Fig. 4a). This implies that IC itself was hardly decomposed by visible light or H_2O_2. In the other words, significant degradation was observed under visible light irradiation when both GFO and H_2O_2 were present, which suggests GFO as a heterogeneous visible-light-responsive Fenton-like catalyst. The pseudo-first-order model was used to better understand the reaction kinetic of IC degradation *via* different systems:

$$-ln\frac{C_t}{C_0} = kt$$

From the pseudo-first-order kinetic modelling (Fig. 4b), the apparent rate constant k was 2.6×10^{-4}, 9.45×10^{-4}, 0.0048, and 0.0499 min^{-1} for photolysis, H_2O_2/visible light, GFO/visible light, and GFO/H_2O_2/visible, respectively. The highest value of k was observed for GFO/H_2O_2/visible, suggesting the fastest degradation rate and best photocatalytic activity through photo-Fenton process. The IC photo-Fenton degradation performance of GFO was promising when compared with literature [16], although note that the reaction conditions varied. For example, GFO removed 98.5 % IC after 90 min visible light irradiation under the conditions of dye concentration = 10 mg/L; catalyst dosage = 1.0 g/L; H_2O_2 concentration = 10 mM; solution pH = 6, and temperature = 25 °C. In addition, under the similar conditions (initial dye concentration = 10 mg/L; photocatalyst dosage = 1.0 g/L; initial H_2O_2 concentration = 10 mM), the $LaFeO_3$ supported polymer resin only degraded 60 % IC after 170 min visible light irradiation [16].

Mechanism of photo-Fenton catalysis to decompose organic pollutants in wastewater under visible light radiation of GFO photocatalyst can be proposed to occur through two processes at the same time, it is the Fenton reaction and the photocatalysis process, specifically as follows: During the Fenton reaction, the Fe atom on the surface of the GFO material (FeIII) can react with H_2O_2 to generate hydroxyl radicals ▪OH (Eqs. 2-5):

$$Fe^{III} + H_2O_2 \rightarrow Fe^{III}H_2O_2 \ (2)$$

$$Fe^{III}\ H_2O_2 \rightarrow Fe^{II} + HO_2\blacksquare + H^+ \ (3)$$

$$Fe^{III} + HO_2\blacksquare + H^+ \rightarrow Fe^{II} + O_2 + 2H^+ \ (4)$$

$$Fe^{II} + H_2O_2 \rightarrow Fe^{III} + \blacksquare OH + OH^- \ (5)$$

https://doi.org/10.62239/jca.2024.020

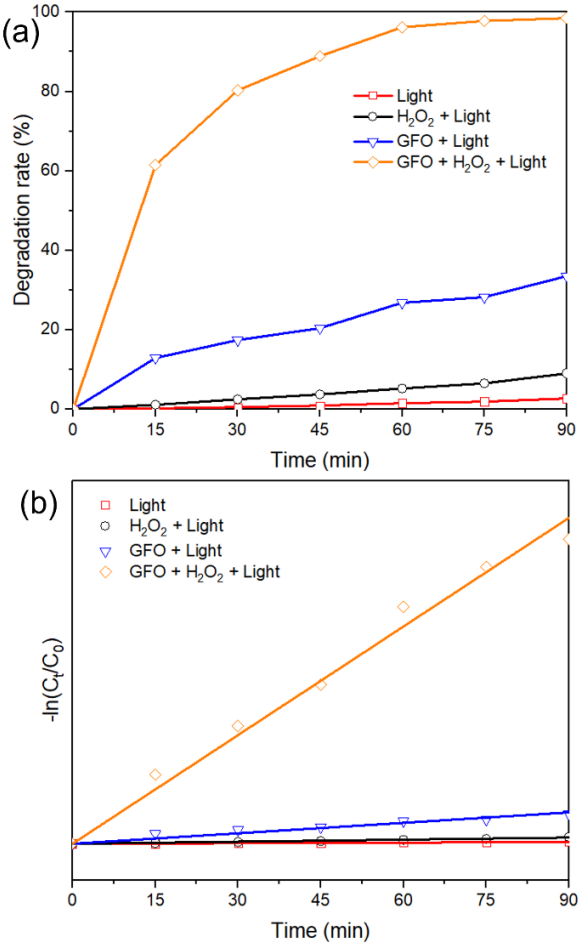

Fig 5: (a) Photo-Fenton degradation of IC as a function of irradiation time by using GFO (reaction conditions: dye concentration = 10 mg/L; catalyst dosage = 1.0 g/L; H_2O_2 concentration = 10 mM; solution pH = 6; temperature = 25 °C); and (b) plots of -ln (C/C_0) versus irradiation time

These free radicals will directly oxidize organic compounds present in wastewater to form degradation products [21].

Meanwhile, the photocatalysis reaction begins when the GFO molecules absorb photons with energies greater than its band gap from the emitted light. From there, the electrons will be excited and move from the valence band (VB) to the conduction band (CB) and at the position where the electrons are ejected creating holes (h+) with positive and negative charges (e-) on the GFO surface (Eq. 6). These (e-) will then be trapped by H_2O_2 molecules and also generate ▪OH free radicals (Eq. 7) [22]. Thus, free radicals are continuously generated and combined with dye molecules to form intermediate compounds through the processes of oxidation, mineralization, etc., leading to their decomposition under the action of visible light (Eq. 8), as follows:

$$GFO \rightarrow GFO\ (e^- + h^+)\ (6)$$

$$H_2O_2 + e^- \rightarrow \cdot OH + OH^-\ (7)$$

$$\cdot OH + dye \rightarrow \text{Degradation products}\ (8)$$

4. Conclusions

$GdFeO_3$ material (GFO) has been successfully synthesized by hydrothermal method using citric acid as a chelating agent. GFO has quite high photo-Fenton catalytic activity, which can decompose organic dye (Indigo Carmine) from wastewater, achieving degradation efficiency of 98.5 % after 90 min, higher than that of GFO material *via* photocatalysis. The improvement of photocatalytic activity is attributed to the combination of high photocatalysis capacity and good Fenton photocatalytic activity of GFO material. The results suggest that GFO is as a promising heterogeneous visible-light-responsive Fenton-like catalyst for degradation of dye from wastewater.

Acknowledgement

This research is funded by Vietnam National Foundation for Science and Technology Development (NAFOSTED) under grant number 104.05-2020.06.

References

1. M. Rodriguez, V. Sarria, S. Esplugas, C. Pulgarin, J. Photochem. Photobio. A: Chem. 151(1-3) (2002) 129-135. https://doi.org/10.1016/S1010-6030(02)00148-X
2. A.H. Jawad, A.S. Abdulhameed, M.S. Mastuli, J. Taibah Uni. Sci. 14(1) (2020) 305-313. https://doi.org/10.1080/16583655.2020.1736767
3. D. Bhatia, D., N.R. Sharma, J. Singh, R.S. Kanwar, Cri. Rev. Environ. Sci. Technol. 47(19) (2017) 1836-1876. https://doi.org/10.1080/10643389.2017.1393263
4. U.Y. Qazi, R. Iftikhar, A. Ikhlaq, I. Riaz, R. Jaleel, R. Nusrat, R. Javaid, Environ. Sci. Pollu. Res. 29(59) (2022) 89485-89497. https://doi.org/10.1007/s11356-022-21879-3
5. H. Ahmad, M. Zahid, Z.A. Rehan, A. Rashid, S. Akram, M.>.H. Aljohani, S.K. Mustasfa, T. Khalid, N.R. Abdelsalam, R.Y. Ghareeb, M.S. AlHarbi, Membranes 12(2) (2022) 224. https://doi.org/10.3390/membranes12020224
6. H. Lachheb, E. Puzenat, A. Houas, M. Ksibi, E. Elaloui, C. Guillard, J.M. Herrmann, Appl. Catal. B: Environ. 39(1) (2002) 75-90. https://doi.org/10.1016/S0926-3373(02)00078-4
7. T.T.N.Phan, T.T.N. Phan, T.H. Pham, J. Porous Mater. (2022) 1-12. https://doi.org/10.1007/s10934-022-01378-z
8. T.T.N. Phan, A.N. Nikoloski, P.A. Bahri, D. Li, J. Environ. Chem. Eng. 6(1) (2018) 1209-1218. https://doi.org/10.1016/j.jece.2018.01.033

9. K. Rusevova, R. Koferstein, M. Rosell, H.H. Richnow, F.D. Kopinke, A. Georgi, Chem. Eng. J. 239 (2014) 322-331. https://doi.org/10.1016/j.cej.2013.11.025
10. L. Li, D. Zhang, X. Wei, L. Pan, L. Chen, J. Rong, J. Phys. Chem. Solids, (2023) 111285. https://doi.org/10.1016/j.jpcs.2023.111285
11. Y. Sim, I. Yang, D. Kwon, J.M. Ha, J.C. Jung, Catal. Today, 352 (2020) 134-139. https://doi.org/10.1016/j.cattod.2019.10.038
12. W. Haron, A. Wisitsoraat, S. Wongnawa, Ceram. Intern., 43(6) (2017) 5032-5040. https://doi.org/10.1016/j.ceramint.2017.01.013
13. D. Navas, D., S. Fuentes, A.C. Alvarez, E.C. Angel, Gels, 7(4) (2021) 275. https://doi.org/10.3390/gels7040275
14. S. Wang, X. Wang, L. Yuan, G. Ma, J. Zhang, Y. Zhang, X. Cui, X. Wu, D. Lu, Crys. Growth Design, 20(4) (2020) 2123-2128. https://doi.org/10.1021/acs.cgd.9b01319
15. K. Abdouli, W. Cherif, E. kadri, K. Dhahri, P.R. Prezas, M.P.F. Graca, M.A. Valent, L. Ktari, J. Alloys Compds, 739 (2018) 1048-1058. https://doi.org/10.1016/j.jallcom.2017.12.269
16. A. Alpay, Ö. Tuna, E.B. Simsek, Environ. Technol. Innov., 20 (2020) 101175. https://doi.org/10.1016/j.eti.2020.101175
17. I.R. Parrey, Bulgarian J. Phys., 48(3) (2021).
18. S. Hui, X. Jiayue, W. Anhua, J. Rare Earths 28(3) (2010) 416-419. https://doi.org/10.1016/S1002-0721(09)60124-1
19. I.H. Lone, H. Khan, A.K. Jain, J. Ahmed, K.V. Ramanujachary, T. Ahmad, ACS omega, 7(38) (2022) 33908-33915. https://doi.org/10.1021/acsomega.2c02809
20. Y. Albadi, M.S. Ivanova, L.Y. Grunin, K.D. Martinson, M.I. Chebanenko, S.G. Izotova, V.N. Nevedomskiy, R.S. Abiev, V.I. Popkov, Inorganics, 9(5) (2021) 39. https://doi.org/10.3390/inorganics9050039
21. T.T.N. Phan, A.N. Nikoloski, P.A. Bahri, D. Li, Appl. Surf. Sci. 491 (2019) 488-496. https://doi.org/10.1016/j.apsusc.2019.06.133
22. T. Huang, J. Zhu, S. Ge, T. Guo, C. Jiang, L. Xie, J. Environ. Chem. Eng. 8(5) (2020) 104384. https://doi.org/10.1016/j.jece.2020.104384